REPORT DOCUMENTATION PAGE

Form Approved
OMB No. 0704-0188

Public reporting burden for this collection of information is estimated to average 1 hour per response, including the time for reviewing instructions, searching existing data sources, gathering and maintaining the data needed, and completing and reviewing this collection of information. Send comments regarding this burden estimate or any other aspect of this collection of information, including suggestions for reducing this burden to Department of Defense, Washington Headquarters Services, Directorate for Information Operations and Reports (0704-0188), 1215 Jefferson Davis Highway, Suite 1204, Arlington, VA 22202-4302. Respondents should be aware that notwithstanding any other provision of law, no person shall be subject to any penalty for failing to comply with a collection of information if it does not display a currently valid OMB control number. **PLEASE DO NOT RETURN YOUR FORM TO THE ABOVE ADDRESS.**

1. REPORT DATE *(DD-MM-YYYY)*	**2. REPORT TYPE**	**3. DATES COVERED** *(From - To)*
20-08-2009	Technical Paper	

4. TITLE AND SUBTITLE

Quartz Crystal Microbalance Based System for High-Sensitivity Differential Sputter Yield Measurements

5a. CONTRACT NUMBER

5b. GRANT NUMBER

5c. PROGRAM ELEMENT NUMBER

6. AUTHOR(S)

J.L. Topper, B. Rubin, C.C. Farnell , & A.P. Yalin (Colorado State University)

5d. PROJECT NUMBER

5e. TASK NUMBER

5f. WORK UNIT NUMBER

33SP0853

7. PERFORMING ORGANIZATION NAME(S) AND ADDRESS(ES)

Air Force Research Laboratory (AFMC)
AFRL/RZST
4 Draco Drive
Edwards AFB CA 93524-7160

8. PERFORMING ORGANIZATION REPORT NUMBER

AFRL-RZ-ED-TP-2009-318

9. SPONSORING / MONITORING AGENCY NAME(S) AND ADDRESS(ES)

Air Force Research Laboratory (AFMC)
AFRL/RZS
5 Pollux Drive
Edwards AFB CA 93524-7048

10. SPONSOR/MONITOR'S ACRONYM(S)

11. SPONSOR/MONITOR'S NUMBER(S)

AFRL-RZ-ED-TP-2009-318

12. DISTRIBUTION / AVAILABILITY STATEMENT

Approved for public release; distribution unlimited (PA #09384).

13. SUPPLEMENTARY NOTES

For 31st International Electric Propulsion Conference (IEPC 09) to be held in Ann Arbor, MI from 20-24 September 2009.

14. ABSTRACT

We present a quartz crystal microbalance (QCM) based system for high sensitivity differential sputter yield measurements of different target materials due to ion bombardment. The differential sputter yields can be integrated to find total yields. Possible ion beam conditions include ion energies in the range of 30-350 eV and incidence angles of 0-70o from normal. A four-grid ion optics system is used to achieve a collimated ion beam at low energy (<100 eV) and a two grid ion optics is used for higher energies (up to 750 eV). A complementary weight loss approach is also used to measure total sputter yields. Validation experiments are presented that confirm high sensitivity and accuracy of sputter yield measurements.

15. SUBJECT TERMS

16. SECURITY CLASSIFICATION OF:			**17. LIMITATION OF ABSTRACT**	**18. NUMBER OF PAGES**	**19a. NAME OF RESPONSIBLE PERSON**
					Justin Koo
a. REPORT	**b. ABSTRACT**	**c. THIS PAGE**	SAR	17	**19b. TELEPHONE NUMBER** *(include area code)*
Unclassified	**Unclassified**	**Unclassified**			N/A

Standard Form 298 (Rev. 8-98)
Prescribed by ANSI Std. 239.18

Quartz Crystal Microbalance Based System for High-Sensitivity Differential Sputter Yield Measurements (PREPRINT)

IEPC-2009-045

J.L. Topper, B. Rubin, C.C. Farnell, A.P. Yalin

Dept. of Mechanical Engineering, Colorado State University, Fort Collins, Colorado, 80523,USA

We present a quartz crystal microbalance (QCM) based system for high sensitivity differential sputter yield measurements of different target materials due to ion bombardment. The differential sputter yields can be integrated to find total yields. Possible ion beam conditions include ion energies in the range of 30-350 eV and incidence angles of 0-70° from normal. A four-grid ion optics system is used to achieve a collimated ion beam at low energy (<100 eV) and a two grid ion optics is used for higher energies (up to 750 eV). A complementary weight loss approach is also used to measure total sputter yields. Validation experiments are presented that confirm high sensitivity and accuracy of sputter yield measurements.

I. Introduction

Sputtering, the erosion of a target material under particle bombardment, first discovered in the middle of the nineteenth century, is still an area of active research[1]. Much of the experimental work aims to measure the total sputter yield; however, the angular distribution of sputtered particles, or differential sputter yield, is also of great interest from both fundamental and applied points of view. Differential sputter yield measurements are important for better theoretical understanding of atomic-scale collision and emission processes[1] and are also of practical interest in areas such as sputter deposition[2] and space electric propulsion (EP)[3-14]. In the former, knowledge of the angular distribution of sputtered material is essential for optimization of manufacturing processes. In the latter, angular distributions are necessary to analyze re-deposition of potentially damaging material sputtered by energetic ions from plasma thrusters, for example deposition of sputter products onto solar panels or thermal control surfaces can compromise spacecraft operation. Furthermore, the sputtering in many EP thrusters is predominantly due to low energy ions (~30-100 eV)[13,14] for which the corresponding sputter yields are relatively low (<~1 atom/ion in atom based units). Therefore, the ability to make sensitive differential sputter yield measurements at low energies is critical.

Total sputter yields can be measured using weight loss[15], profilometry[16], quartz crystal microbalance (QCM)[4-5,17-19], and optical emission spectroscopy (OES)[20]. The high sensitivity of the OES and QCM techniques allow sputter yield measurements at low ion energies near the sputtering threshold. Total sputter yield measurements of argon ions on gold were measured using the QCM technique for ion energies of 10-100 eV[18] and total sputter yields of xenon ions on molybdenum, titanium, beryllium and carbon were measured at energies as low as 10 eV using OES[20].

Measurement of differential sputter yields, especially for low ion energies, is more challenging. Differential sputter yields are most commonly measured using collector surfaces[17,21-26] that are used to collect the sputter deposited material, which is later analyzed with different analytical techniques, such as photometry[23], profilometry[25], Rutherford backscattering[27-28], secondary ion mass spectrometry[26,29], electron probe microanalysis[30], radioactive tracer measurements[22] etc. The use of collector plates

precludes *in situ* measurements. Other methods, such as quartz crystal microbalance[6-8,10-12,31-33], mass spectrometry[34-36], laser-induced fluorescence (LIF)[37], and cavity ring-down spectroscopy (CRDS) [38,39], also used for differential sputter yield measurements, are free from this disadvantage. A disadvantage of the mass spectrometry technique is its significant geometric limitations. Mass spectrometers are usually mounted at a fixed location relative to the vacuum chamber, which limits the ability to measure full angular distribution of the sputtered material[43]. The optical techniques of LIF and CRDS are both attractive owing to their non-intrusive nature, but have limitations, for example the need to match the wavelength of the laser source to the species being studies. QCM based studies are further discussed below. Unlike total sputter yields which have been measured at ion energies close to the sputter threshold for some ion – target combinations, there is a paucity of differential sputter yield data for low energy ions (<~100 eV). The majority of studies have been performed in the ion energy range of about one thousand electron volts and above [21,26,37], though some studies have also been performed at the lower energies i.e. 50-1000 eV [35,36,40,41].

In general, experimental results of differential sputter yields obtained at energies above ~1 keV are in good agreement with prediction of Sigmund's theory, i.e. sputter yields with no azimuthal dependence and simple $\cos(\alpha)^n$ dependence where α is the polar ejection angle and n is a constant greater than unity for over cosine-profiles and less than unity for under-cosine profiles. Approximating such profiles with a simple diffuse form proportional to $\cos(\alpha)$ may be adequate in some cases. On the other hand, for energies below ~300 eV systematic deviations from Sigmund's theory have been observed[8,42]. These profiles (for non-normal incidence) tend to exhibit complex shapes that additionally depend on the azimuthal angle, typically with increased sputtering in the forward direction and reduced sputtering in the backward direction. (Full geometric definitions can be found in the aforementioned references but, approximately speaking, the backward direction is back towards the incident ion direction while the forward direction is that corresponding to specular reflection of the ion.) In such cases the use of a diffuse profile does not provide adequate description and full measurement is critical.

As mentioned above, QCM based systems can be used for both total and differential sputter yield measurements. When the QCM is used for total sputter yield measurements, its surface is coated with the target material, and then bombarded by the ions to measure the mass removal rate, which is proportional to the sputter yield. In contrast, for differential sputter yield measurements, the QCM is used in deposition mode meaning that it acts as a collector surface and is coated by particles sputtered from the target. Instead of a single measurement of mass removal rate, the mass deposition rate is measured at multiple sputtering (ejection) angles by scanning the QCM above the sputtering target. Only a limited solid angle is collected at each location (typically about 1/100th of hemisphere) so that higher sensitivity in the rate of mass change is required for given ion/target conditions. The mass deposition rates allow calculation of the differential sputter yield at the corresponding angle, and a series of such measurements can be used to describe the full differential sputter yield profile. The differential sputter yield can, of course, be integrated to give the total sputter yield. Compared to other experimental methods used to measure differential sputter yield measurements, the QCM approach has several advantages including the possibility to perform *in situ* measurements, high cost efficiency, and relative simplicity. In our apparatus, in order to measure differential sputter yields with reasonable angular resolution at low ion energies as is needed for EP, we have focused on high sensitivity. The system can measure mass deposition rates as low as $\sim 10^{-5}$ g/C allowing, for example, differential sputter yields for ion energies as low as 60 eV for Xe ions on BN which, as described above, is critical to EP applications. In contrast, past work using QCMs for differential sputter yield measurements has been primarily at higher energies[8,32,33].

Sputter yield measurements at low ion energies require appropriate ion sources. For example, past work using QCM sensors employed a magnetron as an ion source[32,33]. The advantage of the ion source described in this contribution compared to the magnetrons from the studies mentioned above is that the ion source allows one to obtain nearly monoenergetic ion beams over a wide energy range (from near-threshold energy to hundreds of electron volts) and with different ion incidence angles relative to the target (while magnetron sputtering is always at normal incidence). The ion beam also has very well-defined properties, including low beam divergence, narrow energy spread, and low doubly charged ion fraction, which are essential for high accuracy differential sputter yield measurements.

In this contribution we describe a quartz crystal microbalance (QCM) based experimental system for high sensitivity differential sputter yield measurements in the ion energy range of 30 to 750 eV. The measurement approach uses a combination of weight-loss and QCM deposition sensor techniques[6-8,10-12]. In Section II we discuss the experimental apparatus, while Section III presents measurement and data analysis procedures. Validation and demonstrative measurements illustrating the sensitivity and the accuracy of the experimental system are presented in Section IV. These results include total and

differential sputter yields of gold under bombardment by xenon ions at ion energies range of 30-350 eV and at incidence angles 0-67.5°. Conclusions are given in Section V.

II. Experimental apparatus

A. Description of Sputter Measurement System

A quartz crystal microbalance (QCM) deposition monitor is used to measure differential sputter yields. Total sputter yields can be found by integrating the differential sputter yield profile and are also directly measured using a weight loss approach. A schematic of the experimental apparatus is shown in Fig. 1. The main elements of the system have been previously described[6-8, 10-12]. In this subsection we give an overview of its essential features, while the following subsections detail specific aspects and modifications. Improvements relative to our past work[8] that enable measurements at low ion energies and yields include use of a new four-grid ion source, higher accuracy temperature control, and use of a new QCM crystal and controller. The new source allows a collimated monoenergetic beam at the needed ion energies while the other modifications reduce measurement noise thereby allowing significantly improved sensitivity critical to obtaining low energy yields. The ion source and QCM are housed within a 0.125 m^3 stainless steel vacuum chamber (43 cm ID x 76 cm long main section), equipped with a 1500 liter/s cryogenic pump (CTI-8). The chamber base pressure is 5×10^{-5} Pa giving a working pressure of approximately 0.6 to 1.3×10^{-2} Pa. The DC four-grid ion source is specially designed for low energy operation and is described below in more detail. A rotatable target-mount is positioned 23 cm downstream of the ion source. Both QCM and target rotation are performed using 25000 step stepper motors controlled using a motion control system (Parker CompuMotor). A personal computer (LabView) is used for controlling the QCM and target rotation and for data logging. Detailed discussion of the QCM sensor is provided in Section IID.

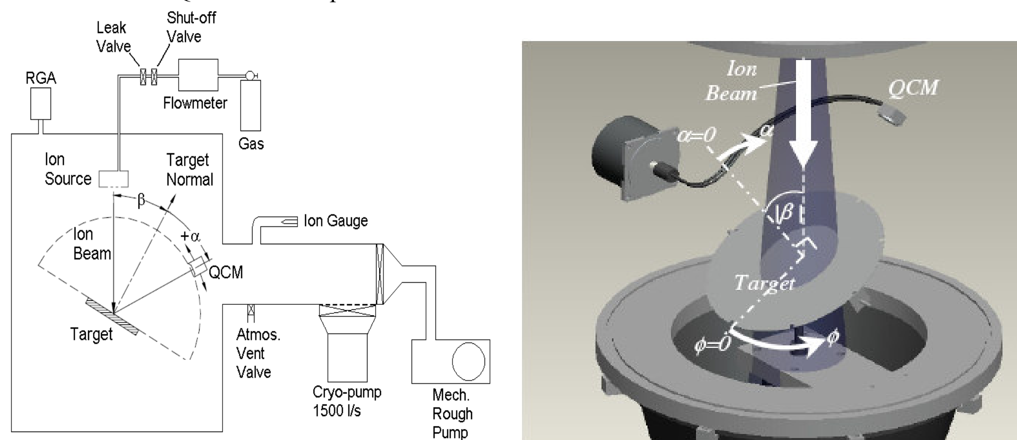

Figure 1. Schematic diagram of the experimental set-up.

B. Four-Grid Ion Source

For measurements at low ion energies a DC ion source with a dual thoriated tungsten filament as a discharge cathode and thoriated tungsten filament as a neutralizer is used[12]. The four-grid ion optics system, designed using our in-house ffx code[44] and fabricated in-house, enables collimated beams at the low ion energies of interest to this work (30-350 eV). The grids have diameter of 3 cm and are manufactured from Poco graphite. For higher energy (250-1500 eV) measurements an alternative two-grid ion optics system with 2 cm aperture, also manufactured from Poco graphite, can be used. In the energy range of 250-350 eV, both ion optics systems can be used, and the measurement results are consistent between two systems. The ion source can be operated on different noble gases.

The four-grid ion optics includes a screen grid (the innermost), an acceleration grid, a focusing grid, and a deceleration grid (the outermost). The screen grid is used to control the beam energy and is maintained positive to ground, while the acceleration grid draws the ion beam out of the source and is maintained at negative 550-625 V relative to ground. The focus grid collimates the beam, and is held negative to ground, generally at -125 V. Finally, the deceleration grid helps prevent electron backstreaming, and is generally maintained slightly negative (~2 V) relative to ground. A typical xenon flow rate is 0.5 sccm, typical discharge voltage is 20 to 40 volts, and typical neutralizer current is 150% of the beam current.

During sputter measurements the ion current leaving the source is recorded. Figure 2 shows an example of extracted total beam current as a function of the beam voltage. Monitoring the ion source current confirms source operation, but sputter yields are determined from measurements of the current reaching the target (performed before and after the sputter tests). When a conductive target is being sputtered, it is possible to directly measure the current reaching the target. This is particularly important for high incidence angles because, due to beam divergence, some fraction of the ion beam does not reach the target. To measure the target current, the target is biased negative 30 V relative to the reference vacuum chamber ground to repel electrons. For non-conductive targets, the target current can be measured by replacing the target with a metal target of the same size. Determination of the sputter yield requires the current of energetic particles (ions and fast neutrals) incident on the sputtering target. As in our past work[10-12], we make corrections for charge-exchange and scattering. The charge-exchange beam generates fast neutrals which, depending on scattering angles, may bombard the target. The resulting correction is to multiply the measured target current (due to ions) by 1.1 ± 0.05.

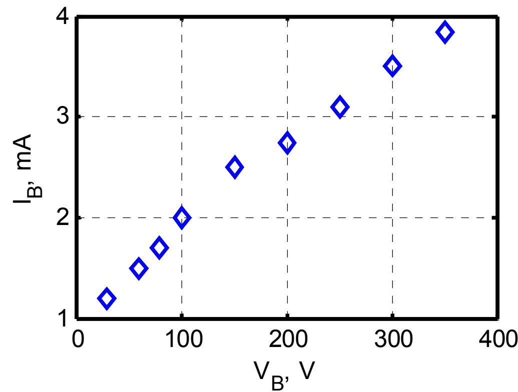

Figure 2. Beam current vs. beam voltage for four-grid ion source optics.

Ion source characterization was performed in order to fully determine the bombardment conditions (ion energy and species composition) with high degree of accuracy. A collimated Faraday probe was used to measure the beam profile, a Retarding Potential Analyzer (RPA) was used to measure the energy distribution of the ions, and an ExB probe was used to measure the ratio of doubly charge ions to singly charge ions.

Ion beam profile

Ion beam profiles were measured using a guarded Faraday probe attached to a rotating QCM mount. The beam full width at half maximum (FWHM) angles found from the beam profiles, are shown in Fig. 3. for several beam voltages. The beam divergence increases as the beam energy is reduced.

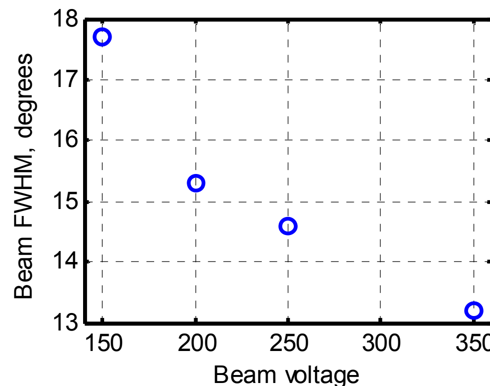

Figure 3. Beam current vs. beam voltage for four-grid ion source optics.

Ion energy distribution

A large area four-grid retarding potential analyzer (RPA) with an aperture diameter of 10.28 cm was used to measure the ion energy distribution[45]. The large diameter increases the sensitivity of the probe, enabling measurements in low density plasma. For the measurements described herein, a

stainless steel mask with a 12.7 mm diameter opening was placed on the RPA. The body of the RPA was made of aluminum and is coated with Alodyne to prevent surface arcing. Several ion energy distribution functions (IEDFs) measured using the RPA are shown in Fig. 4. The peak of the IEDF is located within 2 V of the beam voltage for most operating conditions, and the FWHM is 6-19 volts, increasing with beam energy.

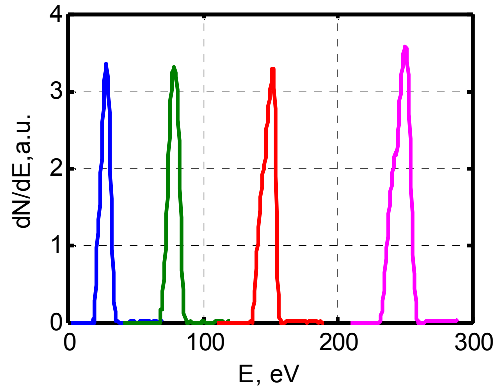

Figure 4. Four different ion energy distributions for beam voltages of 30, 80, 150 and 250 V.

Ion species measurements

The RPA measurements presented above do not discriminate particles by the charge state. To determine the ion species composition, specifically, the ratio of doubly charged ions to singly charged ions, an ExB probe was used. An ExB probe, also known as Wien filter, is a mass spectroscopic device that separates charged particles according to their velocity. The principle of the probe is based on the use of uniform crossed electric and magnetic fields, which are perpendicular to each other and to the particle velocity vector. A schematic of the probe is shown in Fig. 5. Ions passing through a collimator (5 cm long stainless steel tube with 0.5 mm holes on both sides) (1) enter a separation region (2), where the electric (vertical) and magnetic (perpendicular to the picture plane) fields act on it with Lorentz force. When a certain combination of electric and magnetic fields is applied, ions with a corresponding velocity will pass through the separation space and reach the collector (4). The suppressor (3) is used to suppress secondary electron emission from the collector and serves to improve the accuracy of the collector current measurements. During the measurements, the voltage (the electric field) applied between the plates in the separation region is swept, while the collector current is recorded. The dependence of collector current on voltage allows determination of the relative number densities of different ion species, namely, singly and doubly charged xenon ions. In this work, no triple charged ions were detected. An example of ExB probe trace is shown in Fig. 6.

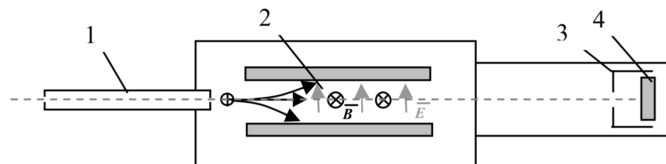

Figure 5. Schematic of ExB probe.

For the four-grid ion source at beam energies between 80 eV and 250 eV the number density ratio of doubly charged to singly charged ions is at most 5%, while for beam energies below 80 eV the number density of doubles is below the detection limit (1%). For a given beam energy, the doubly charged ions possess twice the energy of their singly charged counterparts. As shown in section III, the yield versus energy dependence for the range of energies studied is close to linear, so that doubly charged ions have roughly twice higher sputter yields. In the beam current measurement, each double charged ion is counted as two single charged ions; therefore, owing to the relatively small fraction of double charged ions, their effect on the measured sputter yields is negligible. To prevent the formation of double charged ions during low ion energy measurements (where the effect on measured yields could be more significant), the discharge voltage is reduced below 20 V (i.e. to a value less than the second ionization potential for Xe).

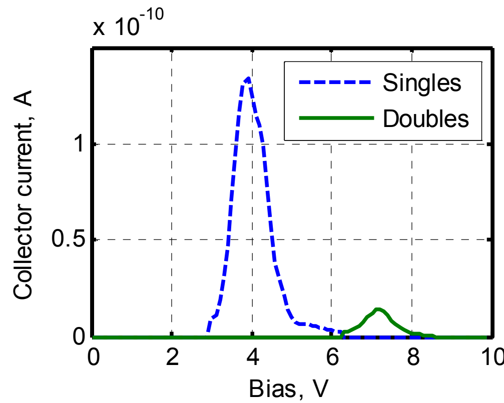

Figure 6. ExB probe trace for an ion beam energy of 250 eV.

C. Surface Charging Effects

Our past measurements of insulator materials such as boron nitride (BN) have shown the effects of surface charging and the importance of appropriate neutralization[10-12]. Similar surface charging effects have been observed by Zhang et al.[46] and Nikiporetz et al.[47]. In order to neutralize the surface charge, a plasma bridge neutralizer (PBN) has been placed in the chamber close to the target. As an example, Fig. 7 shows the dependence of the (apparent) sputter yield of HBC grade boron nitride on beam current, before and after PBN installation.

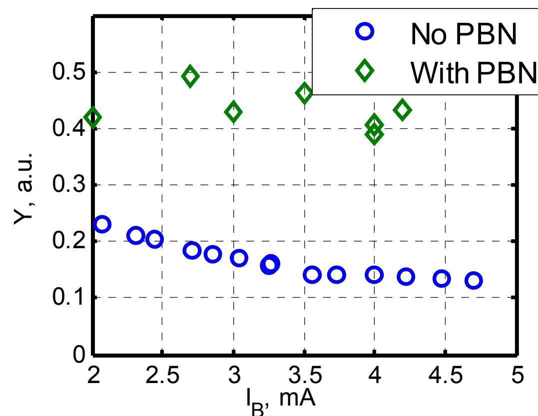

Figure 7. Sputter yield versus beam current with and without PBN installation.

As can be seen in Fig. 7, in the absence of surface neutralization there is a reduction in sputter yield with increasing beam current owing to charge build-up on the BN surface. For higher beam currents, more positive charge is accumulated on the target surface which repels beam ions, thus reducing the measured sputter yield. Measurements of the sputter yield versus beam current with the PBN show a significantly reduced dependence on the beam current since the PBN current neutralizes any surface charge on the target surface. The measurements in Fig. 7 were performed for 500 eV xenon ions at normal incidence with the QCM at 40° (polar angle) from the surface normal. Operating conditions of the PBN included an emission current of 10-20 mA and a Xe mass flow rate of 0.5 sccm. The PBN was biased negatively relative to ground potential.

D. QCM Sensor and Temperature Control

In deposition mode, the QCM allows determination of differential sputter yields through measurement of mass accumulation (of sputtered particles) on its surface. For condensable components, sticking coefficients are assumed to be unity. Sticking coefficients for “new layers” and very thin layers (on the order of several Angstrom) may be less than unity, but once a sufficient layer thickness of a given material has accumulated, sticking coefficients for condensables are generally unity[46]. For the multi-component materials, such as BN, the sputtered particles may consist of a mix of condensable and non-condensable components and data must be interpreted accordingly.

We use a deposition controller (Sigma Instruments SQC-339) that reads the crystal frequency to 0.001 Hz and an RC-cut quartz crystal as opposed to the more conventional AC-cut crystal. The RC-cut crystal (Tangidyne Corporation) is very accurate for deposition of thin films owing to increased sensitivity that is achieved by adjusting the stress coefficients of the quartz plate using advanced fabrication methods. A comparison of measured QCM mass deposition at fixed sputtering conditions using the AC-cut and RC-cut crystals is presented in Fig. 8. The ordinate axis is deposited mass, which (for fixed sputtering conditions) should increase linearly against the charge of ions sputtering the target. The data set measured using the AC-cut QCM has a relatively high noise level, which significantly reduces measurement sensitivity, especially at low ion energies. For most materials of interest, the RC-cut crystal enables measurement of differential sputter yield at ion energies as low as 30-60 eV.

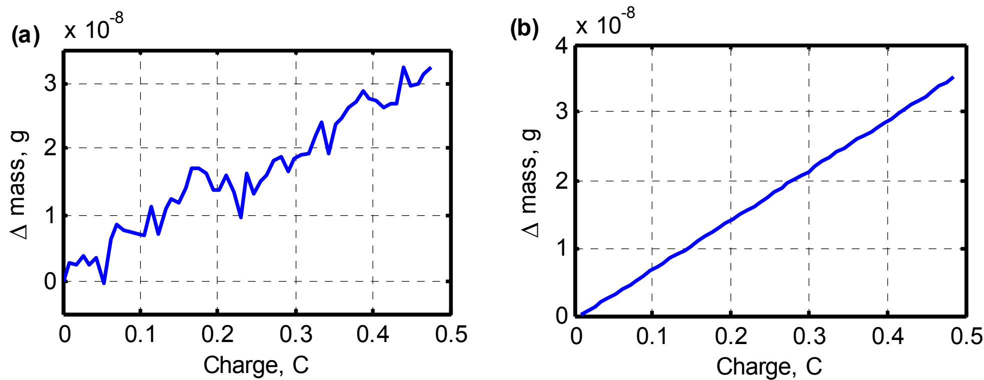

Figure 8. Mass change with AC-cut (left) and RC-cut (right) QCM crystals. Measurement conditions: xenon ions on Quartz at 350 eV, normal incidence, QCM positioned at polar angle of 20°.

The quartz crystal resonance frequency is extremely sensitive to temperature so that for accurate measurements the QCM must be maintained at constant temperature. For this reason cooling water is circulated through the stainless steel body of the QCM housing. Fig. 9 shows the importance of temperature stability, including temperature induced rippling in apparent QCM mass change at fixed sputtering conditions. Again, the ordinate axis is the mass accumulation, the slope of which gives the sputter yield. With lesser temperature stability (±0.1 K), short term rippling is observed and is correlated with temperature variation in the QCM cooling loop. The effect of the rippling is to degrade our ability to determine the slope, thereby degrading overall measurement accuracy and sensitivity. To remedy this behavior we have upgraded to a digital temperature controller (Polyscience 9002) with refrigerating/heating circulator that allows temperature control to ±0.01 K. The right of Fig. 9 shows a similar measurement with the improved temperature controller in which the rippling is significantly reduced leading to improved sensitivity by a factor of approximately 3.

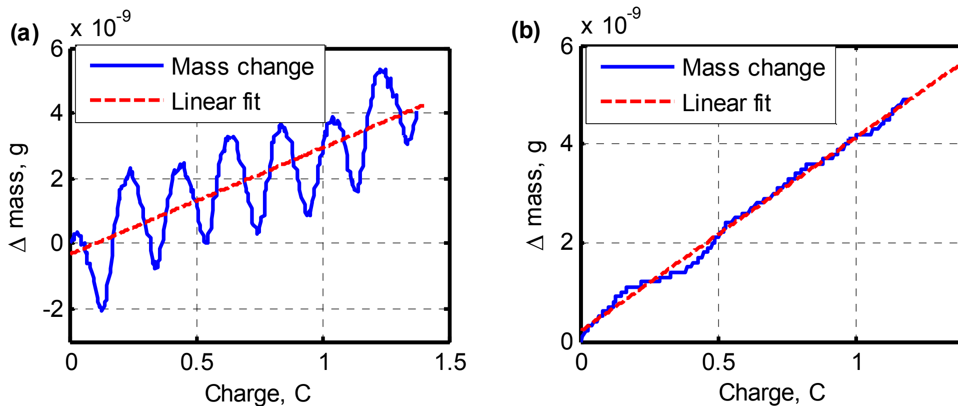

Figure 9. Mass change for temperature controllers with ±0.1 K stability (left) and ±0.01 K stability (right). Measurement conditions: xenon ions on Kapton at 250 eV, incidence angle of 45°, QCM positioned at polar angle of 20°.

As the crystal is moved to different positions during the measurement, its (incoming) heat flux varies due to changes in the relative position of the QCM and the heat sources in the system (ion source and PBN). Therefore, although the temperature of the water stays constant, the actual crystal temperature is different at different locations (polar angles). A K-type thermocouple wire embedded in a copper holder silver-soldered to the back of the QCM crystal holder is used to monitor QCM temperature. When the QCM is moved to each measurement position, the QCM temperature is monitored, and sputter yield measurements are started only after the temperature of the crystal has stabilized.

III. Measurement Procedures and Data Analysis

A. Definition of Angles

The angles used to describe the direction of ion incidence and the ejections angles of sputtered particles are shown in Fig. 1. We define as follows: β is the incidence angle of bombarding ions measured relative to the surface normal (β=0 for normal incidence), α is the ejection polar angle of sputtered atoms measured relative to the surface normal, and ϕ is the ejection azimuthal angle of the sputtered atoms measured in the plane of the target surface (defined so that ϕ=0 is in the forward sputter direction i.e. in the forward direction of the plane containing the surface normal and the incident ion directions).

B. QCM Measurements and Data Analysis

Sauerbrey's equation is used to calculate the mass accumulation rate from the QCM frequency change[49]. A total of 34-36 positions above the target are typically sampled. At a given measurement point the volumetric differential sputter yield, $y(\alpha,\phi)$, in units of mm^3/C/sr, is determined using:

$$y(\alpha,\phi)=\frac{R(\alpha,\phi)r_{QCM}^{2}}{\rho J_{B,avg}A_{s}} \tag{1}$$

where $R(\alpha,\phi)$ is the measured mass accumulation rate (found from a slope of the mass accumulation rate, see Figs. 8-9), ρ is the density of target material, $J_{B,avg}$ (C/s) is the time-averaged current of bombarding particles (ions and energetic neutrals) incident on the target, r_{qcm} is the distance from the target center to the QCM (17.4 cm), and A_s is the QCM sensor area (0.535 cm^2). The quantity A_s/r_{qcm}^2 corresponds to the solid angle that the QCM sensor subtends while $R(\alpha,\phi)/\rho J_{B,avg}$ corresponds to the volume of sputtered material per bombarding charge. It is important to emphasize that the directly measured quantity is the mass buildup of condensable particles on the QCM and the volumetric differential sputter yield should be considered in this way. (In fact the "volume" may not really correspond to any physically observed volume since it corresponds to the equivalent volume due to the mass of the *deposited condensable material* if one uses the density of the full *target material*; of course conversion to the deposited mass yield simply requires removing the density from Eq. (1)).

In principle, because of the finite size of the QCM crystal and beam spot on the target, each of our measurements (i.e. QCM positions) corresponds to a (small) range of polar and azimuthal angles joining the target and QCM. A simple simulation has been performed to show that for our chamber geometry and sputter conditions such effects are negligible (worst case of 5% error), so that the target and QCM can be treated as points (not planes) joined by a single vector[6]. We also note that the viewing angle of the QCM is approximately 5.4 steradians (cone apex angle of 165°) which corresponds to viewing area on the target that is larger than the irradiated area (also a necessary requirement for Eq. (1)). Experimental uncertainty and error bars on measured differential sputter yields are found by estimating individual contributions and combining them to acquire a typical value of ± 16%.

As mentioned above, the accuracy and sensitivity of QCM measurements is limited by temperature drift and fluctuations, which cause drift and fluctuation of the QCM signals. The typical drift rate of the QCM signal was measured when the QCM temperature controller and the ion beam were running but no sputtered material was deposited on the QCM. The fluctuations of the QCM signal due to the thermal perturbations are on the order of $1\text{x}10^{-11}$ g/s. From Eq.(1) it is obvious that, depending on the density of the material and the beam current, this fluctuation can correspond to different error margin and sensitivity threshold in terms of the sputter yield. Using gold as an example of high density material (19.3 g/cm^3) and with a high current value (3 mA), we obtain an error margin of $1\text{x}10^{-4}$ g/C/sr,

which is about two orders of magnitude lower then the actual signal due to the sputtering. In this case thermal drift is insignificant and the accuracy is determined by the other factors. Using BN as an example of low density material (2 g/ cm^3), and with a low current value (1mA), we obtain a value of $3x10^{-3}$ g/C/sr, which in this case will determine the sensitivity threshold of sputter yield measurements. The rated sensitivity of the QCM is least one order of magnitude better that the sensitivities given above and work is underway aimed at achieving better thermal stability of the QCM; however, the present levels are adequate for many measurement needs, even for low energy sputtering.

C. Modified Zhang Equations

Analysis and fitting of differential sputter yield profiles requires appropriate functional forms. At our conditions, stopping is predominantly due to elastic (nuclear) collisions and is generally in the linear cascade regime (emitted particles are secondary or higher generation recoils) or single knock-on regime (emitted particles are primary recoils)[1]. A classical theory for the linear cascade regime was originally developed by Sigmund[50]. Independent of ion incidence angle, the original Sigmund theory predicts sputtering profiles that are azimuthally symmetric and approximately diffuse in shape, corresponding to cosine-like profiles of the form $y \propto \cos(\alpha)^n$ (n=1 for a diffuse profile). More recent experimental and numerical studies show a range of profile shapes. For normally incident ions on polycrystalline and amorphous targets, cosine-like profiles are generally observed with increasingly under-cosine shapes as ion energy is lowered and increasingly over-cosine shapes for higher ion energies[6-8,10-12,23,51,52]. For obliquely incident ions at relatively high ion energy, observed profiles also tend to be azimuthally symmetric. However, for lower ion energies the measured profiles tend to be asymmetric with increased sputtering in the forward direction[6-8,10-11,22,23,31]. Similar profiles have been modeled on a theoretical basis[52-54].

As a means to describe the measured differential sputter yield profiles we use expressions from Zhang[42], based on work from Yamamura [53-54], to which we introduce two fit parameters. We term the resulting expressions as Modified Zhang (MZ)[8]:

$$y_{MZ} = \frac{Y}{1-\sqrt{\frac{E^*}{E}}\cos(\beta)} \cdot \frac{\cos(\alpha)}{\pi}\left[1-\frac{1}{4}\sqrt{\frac{E^*}{E}}\left(\cos(\beta)\gamma(\alpha)+\frac{3}{2}\pi\sin(\beta)\sin(\alpha)\cos(\phi)\right)\right], \quad (2a)$$

$$\gamma(\alpha) = \frac{3\sin(\alpha)^2-1}{\sin(\alpha)^2} + \frac{\cos(\alpha)^2\left(3\sin(\alpha)^2+1\right)}{2\sin(\alpha)^3}\ln\left(\frac{1+\sin(\alpha)}{1-\sin(\alpha)}\right), \quad (2b)$$

where y_{MZ} is the differential sputter yield, Y is the total sputter yield, E is the ion energy, E^* is a characteristic energy describing the profile shape, and the angles are as defined above. The approach decouples the amplitude of the angular profiles from their shape, through the use of Y and E^* respectively. More recent work by Zhang[46] also discusses the use of a varying energy parameter. In general, rather than using the MZ expressions for *a priori* calculation, we treat Y and E^* as free fit-parameters which we determine from (least-squares fitting) experimental data. Determining the total yield in this way is roughly equivalent to integrating the differential sputter yield profiles. Note that profile shapes are determined by the ratio E^*/E and for high ion energy ($E^*/E \ll 1$) the MZ expression reduces to the diffuse yield ($y = Y\cos(\alpha)/\pi$). A least-squares algorithm (realized in MATLAB) is used to find the values of Y and E^*. The uncertainty in E^* is calculated from statistical variation between different measurements.

D. Weight Loss Analysis

In some cases we perform weight-loss measurements as a complimentary means to determine total sputter yields. For multi-component materials with sputter products that may contain a mix of condensable and non-condensable species (e.g. BN), comparison of total yields from QCM (which detects only condensables) versus weight-loss (which detects all species) provides additional insight into the identity of sputter products (i.e. the fraction that is condensable). A microgram scale (Mettler AE163) is used to weigh the targets before and after each sputtering session. With this method the volumetric sputter yield, Y (in units of mm^3/C), of each target is found using:

$$Y = \frac{\Delta m}{\rho\, J_{B,Avg}\, t} \quad (3)$$

where Δm represents the mass loss due to ion beam exposure, t is the exposure time, and other symbols are defined as above.

Measurement uncertainties for total sputter yields are calculated by estimating individual contributions and combining them. Uncertainties are as follows: ± 15% on beam current, ± 200 μg on mass measurements, and ±1% on test time lengths. The error on mass tends to dominate at low yields and our mass uncertainty is an order of magnitude larger than that provided by the scales themselves owing to the observed reproducibility in our experiment (see below). The resulting uncertainty in total yields varies depending on measurement conditions, but typical values are approximately 25%. Note that this value is a random error resulting from finite accuracy of the mass, current, and time measurements.

One factor that can affect the weight loss measurement accuracy is moisture absorption by the target materials, for example some grades of boron nitride. When exposed to atmosphere, the targets start absorbing moisture, which increases their weight. In order to minimize this effect, the vacuum chamber is vented with pure nitrogen and the time of atmospheric exposure before the weight measurement is minimized. Another factor that might affect accuracy of the weight loss measurements is xenon ion implantation into the target. If a significant number of xenon ions are implanted in the target, their effect would be to reduce the measured mass loss and the corresponding sputter yield. In order to check the influence of ion implantation in one experiment, X-ray photoelectron spectrometry (XPS) analysis was performed on a BN target (PHI 5800 X-ray photoelectron spectrometer). XPS measurement confirmed that some xenon implantation did occur in a thin near-surface layer with thickness not exceeding a few nanometers. Simple calculation shows the mass contribution from implanted xenon to be negligible compared to the mass change due to sputtered material.

E. Measurement Procedure

Before the measurements, targets are deliberately pre-sputtered to remove any surface layer that could have been formed by contamination or mechanical modification during the manufacturing process. Pre-sputtered surfaces also better represent the conditions found in long-duration electric propulsion operating applications. An order-of-magnitude estimate for the typical dose of incident ions on a target prior to testing is approximately 10^{19} ions/cm^2 (corresponding to thickness of several microns). Target contamination effects in the vacuum chamber are estimated to be negligible, since for typical conditions the flux of ions incident on the target is approximately 10 times higher than the flux of nitrogen (the major contaminant) to the target[8].

Before placement into the vacuum chamber, targets are placed on the scales described above. Each target is weighed 5 times to ensure stability, and the average value of the measured mass is taken. Targets are then inserted into the vacuum chamber and the sputter measurement is conducted. Test durations are fixed such that the mass change of the test is large compared to the precision of mass measurements, and such that the QCM has time (at each position) to sufficiently stabilize relative to thermal and background noise. Test times vary from less than an hour for higher sputter yield materials (e.g. Mo, Au) and higher energy tests (e.g. 350 eV) to as long as 15 hours for lower sputter yield materials (e.g. BN) and lower energy tests (e.g. 50 eV). After each test, the targets are weighed again and the difference in masses is used for the weight-loss measurement.

IV. Validation measurements

In this section we present validation measurements demonstrating system sensitivity and accuracy. The sputter yield of Xe ions on Au was measured for the ion energy range 30-350 eV and at incidence angles of 0-67.5°. The total yields from weight loss and QCM (found from the Y parameter of the best-fit MZ profile) are self-consistent to within experimental uncertainty. Fig. 10 presents the total yield versus ion energy as well as literature data for comparison[55,56]. The energy dependence is generally in good agreement with the Yamamura and Tawara empiric model[55]. It should be noted that the threshold sputter energy for Xe on Au predicted by Yamamura and Tawara is 19 eV, which is also in broad agreement with our measurements – the lowest energy where sputtering was detected is 30 eV. Both our data and the Yamamura and Tawara predictions are consistently higher than the Wehner and Rosenberg data[56], though similar trends are observed in all cases.

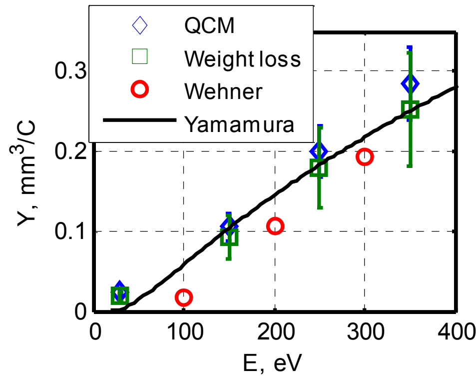

Figure 10. Total sputter yield of gold due to xenon ions at normal incidence.

The dependence of the total sputter yield on ion incidence angle for xenon ions on gold is given in Fig. 11. The sputter yield increases up to incidence angle of 45°, and then drops, which is roughly characteristic for most materials. A prediction from the Yamamura and Tawara model[57] is also given and is in reasonable agreement with our measurements, though the model predicts the peak sputter yield to be at a slightly higher incidence angle.

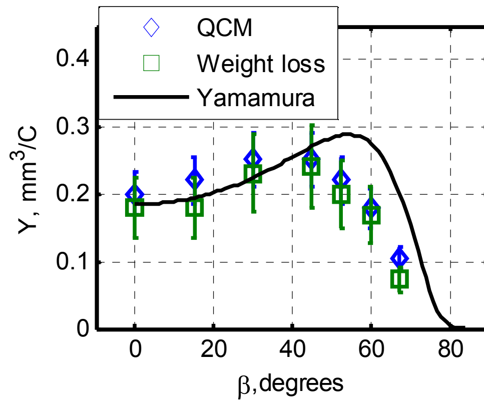

Figure 11. Total sputter yield of gold due to xenon ions versus incidence angle.

Examples of differential sputter yield profiles due to xenon ions on gold are shown in Figs. 12 and 13. Figure 12 shows differential sputter yield profiles for 350 eV ions at normal incidence, and for 250 eV ions at 15° incidence (ϕ=0/180° plane). Experimental data and the corresponding modified Zhang fits are shown, as well as diffuse profiles (with the same total sputter yields) for comparison. For both conditions shown in Fig. 12, as well as for all other conditions studied in this work, the differential sputter yield profiles were significantly non-diffuse, emphasizing the importance of measuring the full angular profiles as opposed to assuming a diffuse shape. For normally incident ions, the observed profiles for the low (≤500 eV) energy ions are typically "under-cosine", meaning reduced sputtering in the normal direction as compared to a diffuse profile, as in Fig. 12a. For non-normal incidence, the profiles are typically azimuthally asymmetric with increased sputtering in the forward (ϕ=0) direction. Fig. 13 shows the hemispheric representation of the differential sputter yield from the best-fit modified Zhang equation for the same two cases.

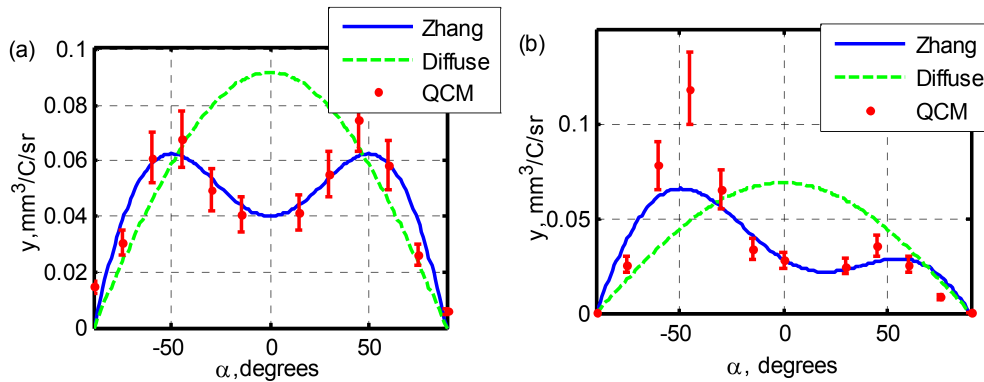

Figure 12. Differential sputter yield profiles xenon ions on gold. (a) 350 eV ions at normal incidence. (b) 250 eV ions at 15° incidence, ϕ=0/180° plane.

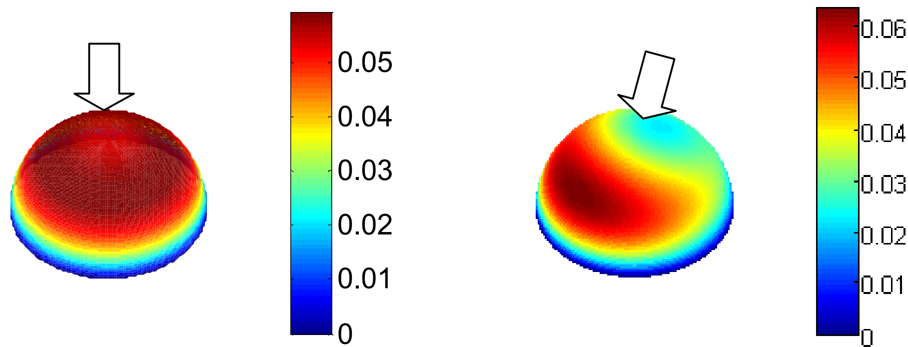

Figure 13. Zhang-fit hemisphere for xenon ions on gold. (left) 350 eV ions at normal incidence. (right) 250 eV ions at 15° incidence, ϕ=0/180° plane. Ion incidence direction is shown with arrow. Differential sputter yields are in units of mm³/C/sr.

The system has been used to measure total and differential sputter yields of a variety materials, including metals (e.g. molybdenum, gold), ceramics (e.g. different grades of boron nitride), polymers (e.g. Kapton), and other multi-component materials (e.g. quartz). Examples of hemispheric representation of the differential sputter yields from the best-fit modified Zhang equation for quartz and Kapton are presented in Fig. 14. For relatively low ion energies (<~500 eV), all studied materials display a non-diffuse differential sputter yield profiles. The energy dependence of the total sputter yields of several materials is given in Fig. 15, demonstrating the wide sensitivity range of the measurement system. Note that the yield values for the multi-component materials in Fig. 15 correspond to QCM-measured yield of condensable components.

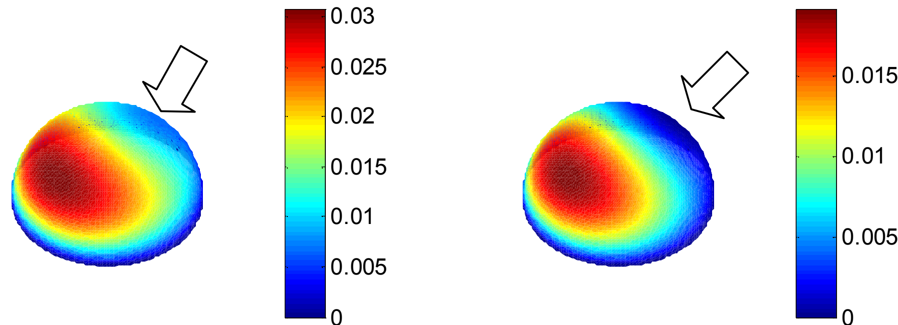

Figure 14. Zhang-fit hemisphere. (left) 350 eV xenon ions on quartz at 30° incidence. (right) 500 eV xenon ions on Kapton at 45° incidence. Ion incidence direction is shown with arrow. Differential sputter yields are in units of mm³/C/sr.

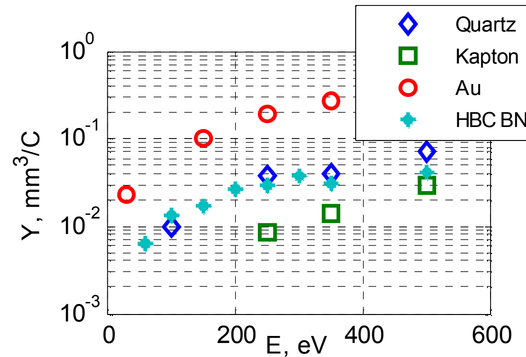

Figure 15. Total sputter yield of Quartz, Kapton, Gold and HBC BN due to xenon ions at normal incidence.

V. Conclusions

We have described a QCM based system used for differential sputter yield measurements. For low ion energies, the system uses a four grid ion source. Source characterizations were presented and show monoenergetic beams with low fractions of multiply charged ions. The QCM employs a high-sensitivity RC-cut crystal to measure the amount of material sputtered in a given angular direction. Scanning the QCM over the hemisphere allows measurement of the full differential sputter yield profile. Temperature stability is found to be critical and a controller with ±0.01 K accuracy is used to stabilize QCM temperature. A plasma bridge neutralizer is used for non-conductive targets to prevent positive charge buildup on the target surface. Validation measurements for Xe ions on Au are presented for ion energies of 30-350eV and incidence angles of 0-67.5^{o}. Total sputter yields from integrating the QCM differential sputter yields are consistent with weight loss measurements and in agreement with published values. Examples of results from other materials are also presented.

Despite the need for low energy (<100 eV) differential sputter yields in a range of applications, there is currently a lack of suitable measurement systems for this purpose. The high-sensitivity and directly quantitative nature of the QCM based system presented here contribute to filling this gap. Differential sputter yield profiles are presented, and for the conditions studied, under-cosine profiles are observed at normal incidence, while profiles with increased forward sputtering are observed for non-normal incidence. In all cases, non-diffuse profiles are observed showing the need to directly measure the angular dependence of the sputter yields.

Acknowledgments

The authors would like to thank the Air Force Research Laboratories (Edwards Air Force Base, CA) and Loral Space Systems for funding support. The authors also thank Paul Wilbur (Colorado State University) for initial development of the QCM apparatus, John Williams (Colorado State University) for assistance with the QCM apparatus and ion source.

References

[1]G. Betz and K. Wien, *J.Mass Spectrom. Ion Proc.* **140,** 1 (1994).

[2]M. A. Vyvoda, C. F. Abrams, and D. B. Grave, *IEEE Trans. Plasma Sci.* **27**, 1433 (1999).

[3]M. Tartz, H. Neumann, B. Fritsche, H. Leiter, and J. Esch, AIAA Pap. **2004**, 4114 (2004).

[4]R. D. Kolasinski, AIAA Pap. **2005**, 3526 (2005).

[5]R. D. Kolasinski, J. E. Polk, D. Goebel, and L. J. Johnson, AIAA Pap. **2006**, 4337 (2006).

[6]K. A. Zoerb, J. D. Williams, D. D. Williams, and A. P. Yalin, Proceedings of IEPC, 2005, 293 (unpublished).

[7]A. P. Yalin, J. D. Williams, V. Surla, J. Wolf, and K. A. Zoerb, AIAA Pap. **2006**, 4336 (2006).

[8]A. P. Yalin, J. D. Williams, V. Surla, and K. A. Zoerb, *J. Phys. D: Appl. Phys.* **40,** 3194 (2007).

[9]J. E. Polk, AIAA Pap. **1999,** 2446 (1999).

[10]A. P. Yalin, B. Rubin, S. R. Domingue, Z. Glueckert, and J. D. Williams, AIAA Pap. **2007**, 5314 (2007).

[11]B. Rubin, J. L. Topper, and A. P. Yalin, Proceedings of IEPC, 2007, 074 (unpublished).

[12]J. L. Topper, B. Rubin, C. C. Farnell, and A. P. Yalin, AIAA Pap. **2008**, 5092 (2008).

[13]S. Cheng, 2002 "Computational Modeling of a Hall Thruster Plasma Plume in a Vacuum Tank", M.Sc. Thesis, Massachusetts Institute of Technology, 2002.

[14]J. Yim, "Computational Modeling of Hall Thruster Channel Wall Erosion" Ph.D. Dissertation, University of Michigan, 2008.

[15]A. P. Yalin, V. Surla, C. Farnell, M. Butweiller, and J. D. Williams, AIAA Pap. **2006**, 4338 (2006).

[16]J. Ustarroz, I. Caro, P. Corengia, I. Garmendia, J. Marcos, E. Ahedo, and J. González del Amo, Proceedings of IEPC, 2007, 167 (unpublished).

[17] P.C. Smith and D.N. Ruzic, *J. Vac. Sci. Technol. A* **17**, 3443 (1999).

[18]D. McKeown, *Rev. Sci. Instr.* **32,** 133 (1961).

[19]G. Hayderer, M. Schmid, P. Varga, H.P. Winter, and F. Aumayr., *Rev. Sci. Instr.,* **70**, 3696 (1999).

[20]R. P. Doerner, D. G., Whyte, and D. M. Goebel, *J. Appl. Phys.* **93**, 5816 (2003).

[21]H. Tsuge and S. Esho, *J. Appl. Phys.* **52,** 4391 (1981).

[22]S. Kundu, D. Ghose, D. Basu, S.B. Karmohapatro, *Nucl. Instr. Meth. Phys. Res. B* **12**, 352 (1985).

[23]G. K. Wehner and D. Rosenberg, *J. App. Phys.* **31,** 177 (1960).

[24]G.S. Anderson, *J. Appl. Phys*. **34**, 659 (1963).

[25]J.-K. Lee, G.-R. Lee, J.-H. Min, and S. H. Moon *J. Vac. Sci. Technol. A* **24**, 1807 (2006) .

[26]C. Verdeil, T. Wirtz, H.-N. Migeon and H. Scherrer, *Appl. Surf. Sci.* **255**, 870, (2008).

[27]V. Shutthanandan, P. Ray, N. Shivaparan, R. Smith, T. Thevuthasan, and M. Mantenieks, Proceedings of IEPC, 1997, 069 (unpublished).

[28]M. Mantenieks, J. Foster, P. Ray, S. Shutthanandan, and T. Thevuthasan, Proceedings of IEPC, 2001, 309 (unpublished).

[29]J. N. Smith, *IEEE Trans. Nucl. Sci.* **26**, 1292 (1979).

[30]T. Aoyama, M. Tanemura, and F. Okuyama, *Appl. Surf. Sci.***100**, 351 (1996).

[31]M. Mannami, K. Kimura, and A. Kyoshima, *Nucl. Instr. Meth.,* **185,** 533 (1981).

[32]C. E. Wickersham and Z. Zhang, *J. Electr. Mat.* **34,** 1474 (2005).

[33]K. Van Aeken, S. Mahieu1, and D. Depla, *J. Phys. D: Appl. Phys.* **41,** 20530 (2008).

[34]A.Wucher, M. Watgen, C.Mobner, H.Oechsner, and B.J. Garrison, *Nucl. Instr. Meth. Phys. Res. B* **67**, 531 (1992).

[35] Oyarzabal, J. H. Yu, R. P. Doerner, G. R. Tynan, and K. Schmid, *J. Appl. Phys.* **100**, 063301 (2006).

[36]E. Oyarzabal, R. P. Doerner, M. Shimada, and G. R. Tynan , *J. Appl. Phys.* **104**, 043305 (2008).

[37]T. J. Whitaker, P. L. Jones, Aijun Li, and R. 0. Watts, *Rev. Sci. Instrum*. **64**, 452 (1993).

[38]V. Surla V and A. P. Yalin, *Appl. Optics* **46,** 3987 (2007).

[39]A. P. Yalin, L. Tao, N. Yamamoto, T. Smith, and A. Gallimore, Proceedings of IEPC, 2007, 075 (unpublished).

[40]C. Doughty, S. M. Gorbatkin, and L. A. Berry, *J. Appl. Phys*. **82**, 1868 (1997).

[41]R. R. Olson, M. E. King, and G. K. Wehner, *J. Appl. Phys.* **50**, 3677 (1979).

[42]Z. L. Zhang and L. Zhang, *Rad. Eff. Def. Sol.* **159,** 301 (2004).

[43]E. Franke, H. Neuman, M. Zeuner, W. Frank, F. Bigl, *Surf. Coat. Technol.* **97**, 90 (1997).

[44]C. Farnell, "Performance and Lifetime Simulation of Ion Thruster Optics", Ph.D. Dissertation, Colorado State University, 2007.

[45]B. Rubin, J. Williams, C. Farnell , J. Vaughn, T. Schneider, and D. Ferguson, *Plasma Sources Sci. Technol.* **18,** 025015 (2009).

[46]L. Zhang and Z. L. Zhang, *Rad. Eff. Def. Sol.* **160,** 337 (2005).

[47]E. Nikiporetz, A. Semenov, I. Shkarban, and E. Khartova, Proceedings of IEPC, 2007, 7 (unpublished).

[48]L. Bachmann and J. J. Shin, *J. Appl. Phys.* **37,** 242 (1966).

[49]C.-S. Lu and O. Lewis, *J. Appl. Phys.* **43***,* 4385 (1972).

[50]P. Sigmund, *Phys. Rev.* **184,** 383 (1969).

[51]T. K. Chini, M. Tanemura, and F. Okuyama, *Nucl. Instr. Meth. Phys. Res. B* **119,** 387 (1996).

[52]Y. Yamamura and K. Muraoka, *Nucl. Instr. Meth. Phys. Res. B* **42,** 175 (1989).

[53]Y. Yamamura, *Rad. Eff. Def. Sol.* **55,** 49 (1981).

[54]Y. Yamamura Y *Nucl. Instr. Meth.* **194,** 515 (1982).

[55]Y. Yamamura and H. Tawara, *At. Data Nucl. Data Tables* **62,** 149 (1996).

[56]D. Rosenberg and G.K. Wehner, *J. Appl. Phys.* **33,** 1842 (1962).

[57]Y. Yamamura, Y. Itikawa, and N. Itoh, "Angular Dependence of Sputtering Yields of Monatomic Solids," *Institute for Plasma Physics Report* IPPJ AM-26, 1983.